Tensor low energy electron diffraction and medium energy ion scattering determination of the Ni(110)*c*(2×2)-Sn surface structure

2002 J. Phys.: Condens. Matter 14 665

(http://iopscience.iop.org/0953-8984/14/4/301)

INSTITUTE OF PHYSICS PUBLISHING JOURNAL OF PHYSICS: CONDENSED MATTER

J. Phys.: Condens. Matter **14** (2002) 665–673 PII: S0953-8984(02)28229-6

Tensor low energy electron diffraction and medium energy ion scattering determination of the Ni(110)$c(2 \times 2)$–Sn surface structure

P D Quinn[1], C Bittencourt[1], D Brown[1], D P Woodruff[1,3], T C Q Noakes[2] and P Bailey[2]

[1] Physics Department, University of Warwick, Coventry CV4 7AL, UK
[2] CLRC Daresbury Laboratory, Daresbury, Warrington WA4 4AD, UK

E-mail: d.p.woodruff@warwick.ac.uk

Received 22 August 2001, in final form 30 November 2001
Published 18 January 2002
Online at stacks.iop.org/JPhysCM/14/665

Abstract

The Ni(110)$c(2\times2)$–Sn surface phase has been investigated by the combination of quantitative low energy electron diffraction (LEED) with the aid of tensor LEED multiple scattering simulations, and medium energy ion scattering using 100 keV H^+ incident ions. The structure is found to involve substitution of half of the outermost Ni atoms of the clean surface by Sn atoms, but the resulting single layer NiSn alloy is corrugated, with the Sn atoms being 0.40 ± 0.03 Å higher above the underlying Ni substrate than the outermost Ni atoms. The results are discussed in the context of previous structural studies of similar surface alloy phases; a weak trend for the amplitude of the corrugation in Ni/Sn surface alloys to become smaller as the surface layer packing density reduces may be consistent with previous ideas of the role of the depletion of valence electron density in the surface layer and the associated surface tensile stress.

1. Introduction

It is now widely recognized that surface adsorption invariably leads to some degree of modification of the structure of the underlying surface, and while this sometimes involves only relatively subtle distortions, more radical reconstruction is quite common. One particular form of adsorbate-induced surface reconstruction is that of surface alloy formation, in which the adsorbate atoms occupy substitutional sites in the outermost layer of the surface. Generally, these surface alloy phases have no direct bulk analogue, and in some cases the constituent elements may even be immiscible in the bulk, providing a clear indication of the fundamentally different energetics at the solid surface. Apart from the underlying need to identify which systems involve this substitutional rather than overlayer adsorption, the detailed structural

[3] Author to whom any correspondence should be addressed.

parameters of these surface alloys provide further insight into their nature. In particular, these surface alloys commonly show a surface 'corrugation', with the atoms of the constituent elements having different layer spacings relative to the underlying substrate. We have recently highlighted [1, 2] the fact that the magnitude of these corrugations is typically less that that expected from a simple hard-sphere model using the usual atomic (metallic) radii. We have attributed this in part to a genuine surface effect associated with the reduced valence electron density in the surface layer of a metal due to spill-over into the vacuum, which gives rise to a contraction of the surface layer spacing and the presence of a tensile surface stress. Within a hard-sphere picture, this tensile surface stress reflects a reduction in the effective atomic radius, allowing larger substitutional atoms to be accommodated with less corrugation.

Recently there have been a number of structural studies, by quantitative low energy electron diffraction (LEED) and low energy alkali ion scattering, of surface alloys phases formed by Sn on transition and noble metal surfaces including Pt(111) [3], Ni(111) [4, 5], Cu(111) [4] and Ni(100) [6]. In part these were motivated by the fact that Sn addition to some transition metals provides improved performance in heterogeneous catalysis (see, for example, [7]). These studies have revealed some clear systematics in terms of the amplitude of the corrugation within the surface alloy phases which, consistent with a simple hard-sphere picture, have shown an increasing amplitude of corrugation as the substrate lattice parameter decreased. In addition, however, they have also shown that the effective radii of the substitutional Sn atoms were smaller than expected even relative to bulk alloys of the substrate with Sn, consistent with a surface effect of the type described above. The fact that Sn forms surface alloys on both Ni(111) and Ni(100), however, raises an interesting question. Does it also alloy on the Ni(110) surface, and are there any detectable systematics in the amplitude of the surface corrugation as the surface packing density of atoms changes across this series of substrates? Here we describe the results of a structural investigation of the Ni(110)$c(2 \times 2)$–Sn surface phase, using both quantitative LEED and medium energy ion scattering (MEIS). We show that this surface does, indeed, comprise a surface alloy. The corrugation amplitude of this surface alloy is very similar to that found on Ni(111) and Ni(100), although there is a very weak trend in values which is consistent with that expected on the basis of our simple model of the role of surface electron depletion.

2. Experimental details

The MEIS experiments reported in this paper were performed at the UK National MEIS facility based at Daresbury Laboratory [8–10], while the quantitative LEED data were taken at the University of Warwick. In both laboratories the experiments were conducted using standard ultra high vacuum chambers equipped with a range of facilities for sample preparation and surface characterization operating with typical base pressures of (1–2) $\times$ 10^{-10} Torr. The Ni(110) substrate was initially prepared by x-ray Laue alignment, spark erosion and mechanical polishing. The crystal was then cleaned *in situ* by repeated cycles of sputtering with 1 keV Ar^+ ions and subsequent annealing to 900 K. During the MEIS work, Auger electron spectroscopy (AES) and qualitative LEED observations were used to verify the surface composition and state of long-range order. In the case of the quantitative LEED experiments, x-ray photoelectron spectroscopy (XPS) was used to verify the surface composition.

The Ni(110)$c(2 \times 2)$–Sn surface phase was prepared by depositing Sn from a Knudsen cell operating at 1400 K for 10 min which resulted in a coverage of 0.75 ML; subsequent annealing to 1000 K for 10 min produced a $c(2 \times 2)$ LEED pattern with a coverage confirmed by the MEIS measurements to be 0.5 ML. This general procedure of over-dosing followed by elevated temperature annealing is widely used as a way of obtaining the best ordered surface phases

for these higher atomic number adsorption phases. In the case of the Ni(100)$c(2 \times 2)$–Sn surface phase, some differences have been reported in the detailed structural information obtained from a sample prepared by deposition of the nominal 0.5 ML onto the sample without subsequent higher temperature treatment [6], but it seems likely that these differences were largely attributable to the worse state of long-range order of the surface.

Quantitative LEED measurements of the diffracted beam intensities were recorded from 40 to 400 eV at room temperature using a computer-interfaced Omicron video-LEED system at nominal normal incidence. The exact incidence geometry was adjusted to achieve normal incidence by comparing the intensity-energy spectra of diffracted beams which should be symmetrically equivalent. Intensity-energy spectra were collected for nine integral order and twenty fractional order beams. The symmetry-equivalent beams were then averaged, reducing the data set from a total of 29 beams to nine symmetrically distinct beams, comprising six integral order and three fractional order beams, covering a total energy range of 2352 eV.

The MEIS experimental facility, and the methods of data acquisition and reduction, have been described more fully in earlier publications [9, 10] and more detailed reviews of the MEIS technique, and of our recent applications of it, can be found elsewhere [2, 11, 12]. The basic approach to surface structure determination by MEIS is based on the so-called 'double-alignment' experiment. Incident ion directions are used which correspond to bulk crystallographic directions, causing the atoms in the outermost surface layers to shadow sub-surface atoms so that only a small number of near-surface layers are illuminated. The relative positions of the atoms in these layers are then determined by studying the angular locations of the 'blocking' dips in the scattered signal which results from nearest-surface atoms obscuring the scattered signal from sub-surface atoms. One key feature of the instrument at Daresbury is that the toroidal-sector electrostatic ion energy analyser is fitted with a position-sensitive detector behind a channel-plate multiplier in the output, and this allows the simultaneous collection of energy and angle-resolved data over a range of both of these parameters. Each of these two-dimensional 'tiles' of data can be joined together by taking a series of measurements at different average angular positions and ion pass energies to extend the range of measured angle and energy. The interpretation of the blocking curves (scattered ion intensity as a function of scattering angle) obtained from these raw MEIS data, as in LEED, is based on computational simulations for different structural models.

3. Experimental results and interpretation

An analysis of the quantitative LEED data was based on the standard 'trial-and-error' approach of modelling the experimental data with multiple scattering calculations for a succession of trial structures, albeit aided by automated search algorithms. Specifically, the calculations were performed using the Barbieri/Van Hove symmetrized automated tensor LEED package, with the associated muffin-tin potential and scattering phase shifts being calculated using the Barbieri/Van Hove phase shift package [13, 14]. Five different adsorption sites were considered for the Sn, namely substitutional, hollow, atop, and the short and long bridge sites. New scattering phase shifts were generated for each of the structures of interest to take account of the small changes in valence charge and muffin-tin radii, although the effect of these differences is very small as the scattering is dominated by the ion cores (a key requirement for the essential effectiveness of LEED structure determination). Eight phase shifts were used in the all the original calculations; in a final optimization stage this was increased to twelve to check for any possible problems, but there was no significant improvement in the quality of the fits. The Pendry R-factor (reliability factor) [15] was used to compare theoretical and experimental LEED intensity-energy spectra, and the minimization of this parameter was used

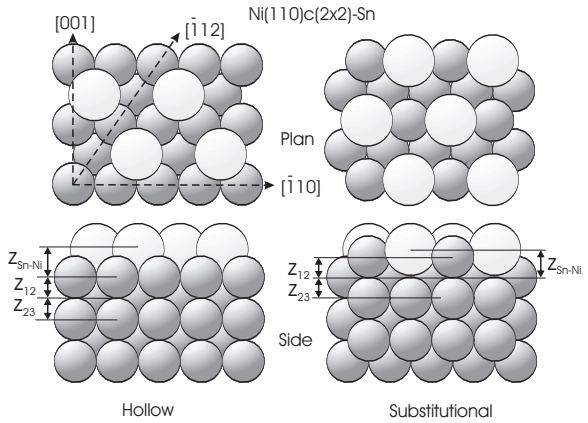

Figure 1. Plan and side views of the substitutional alloy and hollow site overlayer models of the Ni(110)$c(2 \times 2)$–Sn surface phase including a definition of the principle azimuths and the layer spacings determined by the LEED and MEIS experiments.

Table 1. R-factor values for the best fits to each of the different structural models, together with the associated values of the structural parameters, obtained from the tensor LEED analysis. $z_{\mathrm{Sn–Ni}}$ is the layer spacing from the Sn atoms to the last complete Ni layer below. For the overlayer models z_{12} is the spacing of outermost layer Ni atoms to the second layer Ni atoms and z_{23} is the spacing between the second and third layer Ni atoms. For the substitutional alloy model z_{12} is the spacing of the Ni atoms in the alloy layer to the first complete Ni layer and z_{23} is the spacing between the first complete Ni layer and the underlying second complete Ni layer.

Site	R_{p}	$z_{\mathrm{Sn–Ni}}$ (Å)	z_{12} (Å)	Z_{23} (Å)
Substitutional	0.15	0.40 ± 0.03	1.19 ± 0.02	1.26 ± 0.02
Hollow	0.46	1.64 ± 0.07	$1.29 \pm 0.0.3$	1.20 ± 0.03
Atop	0.52	2.95	1.23	1.24
Short bridge	0.69	2.88	1.18	1.30
Long bridge	0.57	1.72	1.19	1.27

as the criterion for the best-fit structures. The Sn atoms were initially placed at layer spacings consistent with hard-sphere models using the atomic radii of the Ni and Sn atoms. The atoms were then allowed to move freely perpendicular to the surface within the constraints of the $c(2 \times 2)$ periodicity and the point group symmetry of the substrate. The vibrational amplitudes of the atoms were initially set to the values implied by the bulk Debye temperatures of 200 K for Sn and 450 K for Ni respectively, but were later refined.

The lowest achievable Pendry R-factors (R_{p}) for each model, and the associated values of the average interlayer spacings, are shown in table 1. Because the $c(2 \times 2)$–Sn structure involves one Sn atom, but two Ni atoms in each substrate layer per primitive unit mesh, these two Ni atoms are symmetrically inequivalent in certain layers and may therefore have different layer spacings. This rumpling possibility was included where it is symmetry-allowed. For the two bridge site models, rumpling of the underlying Ni layers is symmetry forbidden in all layers, but in the atop site model first layer Ni rumpling is allowed, while in the hollow site model second layer rumpling is allowed. In the substitutional site model, the first Ni layer in which rumpling is allowed by symmetry is the third, and such deeper layer distortions were not considered. The first and second layer rumpling of the atop and hollow sites models was found to have very little effect on the overall R-factors for these models. The interlayer spacings

presented in table 1 are the spacings to the averaged layer where rumpling was allowed. Optimization of the non-structural parameter of the imaginary part of the inner potential gave a value of 3.75 eV, while fitting of the vibrational amplitudes yielded values of the effective Debye temperatures for Ni and Sn of 375 and 225 K, respectively. At room temperature this corresponds to root-mean-square (rms) vibrational amplitudes of 0.087 Å for Ni and 0.085 Å for Sn, 40% larger than the values expected for bulk Ni atoms on the basis of the bulk Debye temperature, and broadly consistent with a large scattering contribution from surface layer atoms. Table 1 shows clearly that the substitutional alloy model gives by far the lowest R-factor value of 0.15, with the next lowest value, found for the hollow site overlayer, being 0.46, far outside the variance and easily excluded. Although the LEED analysis shows clearly that the hollow site is not the correct geometry, the precision associated with the optimum values of the structural parameters for this local minimum in the R-factor are shown in table 1 for comparison with the MEIS results described below. Figure 1 shows a schematic diagram of the hollow-site overlayer and substitutional alloy models, defining the principle structural parameters. Figure 2 shows the comparison of the experimental and theoretical intensity-energy LEED spectra for both models. As reflected by the R-factor values, the substitutional alloy model calculations reproduce all the qualitative features of the experimental data, as well as providing a good overall quantitative fit. In contrast, the hollow site overlayer model fails to reproduce many aspects of the experimental data.

MEIS measurements were performed with the sample at room temperature employing 100 keV H^+ incident ions along the $[\bar{1}0\,1]$ direction in the $[\bar{1}\,1\,2]$ azimuth and the $[\bar{1}\,\bar{1}\,2]$ direction in the [001] azimuth, using a sample dose of 4 μC corresponding to approximately 5×10^{15} ions cm^{-2}. The incidence geometries used together with the principle associated blocking directions for the clean surface are illustrated in figure 3. Notice that the $[\bar{1}\,0\,1]$ incident direction nominally illuminates only the outermost layer Ni atoms, while the $[\bar{1}\,\bar{1}\,2]$ incidence illuminates the first and second layers (the even-numbered layers being out of the plane of the odd-numbered layers in this azimuthal plane, as shown in figure 3). However, the effect of thermal vibrations and subtle modifications to the outermost layer spacings means that there is actually significant illumination of several deeper layers in both geometries. For the relatively small scattering angles used here (approximately 50°–80°) the mass difference between Sn and Ni is too small to lead to fully-resolved elastic scattering peaks in the scattered H^+ ion energy spectra. Instead we obtain a partially resolved Sn signal with the signals overlapping at the lowest scattering angles. Blocking curves were therefore obtained by integration of both the Sn and Ni scattering signals over a range of scattered ion energies, corresponding to that expected due to inelastic scattering over a depth corresponding to the first six atomic layers. Complete data sets were obtained by summing blocking curves measured from at least two different freshly-prepared surfaces. The lateral position of the sample was adjusted periodically throughout the data acquisition process to minimize the effect of ion-induced damage to the surface.

Simulations of the experimental blocking curves for different structural models were effected using the VEGAS computer code [16]. A Thomas–Fermi–Moliere scattering potential was assumed for the theoretical calculations which exploited the higher speed of the VEGAS program when the incident and back-scattered ion trajectories are treated independently, thus taking no explicit account of correlations in the random displacements exploited in the Monte Carlo algorithm. The quality of fit between experimental and theoretical data was evaluated by means of a reliability factor (R-factor) based on a χ-squared criterion, as described more fully in earlier papers [2, 10, 17]. The search for the optimum structure as defined by the lowest R-factor was aided by a new automated search procedure which we have recently developed for MEIS [18] based on a quasi-Newton (BFGS) search algorithm [19, 20]. The results of the

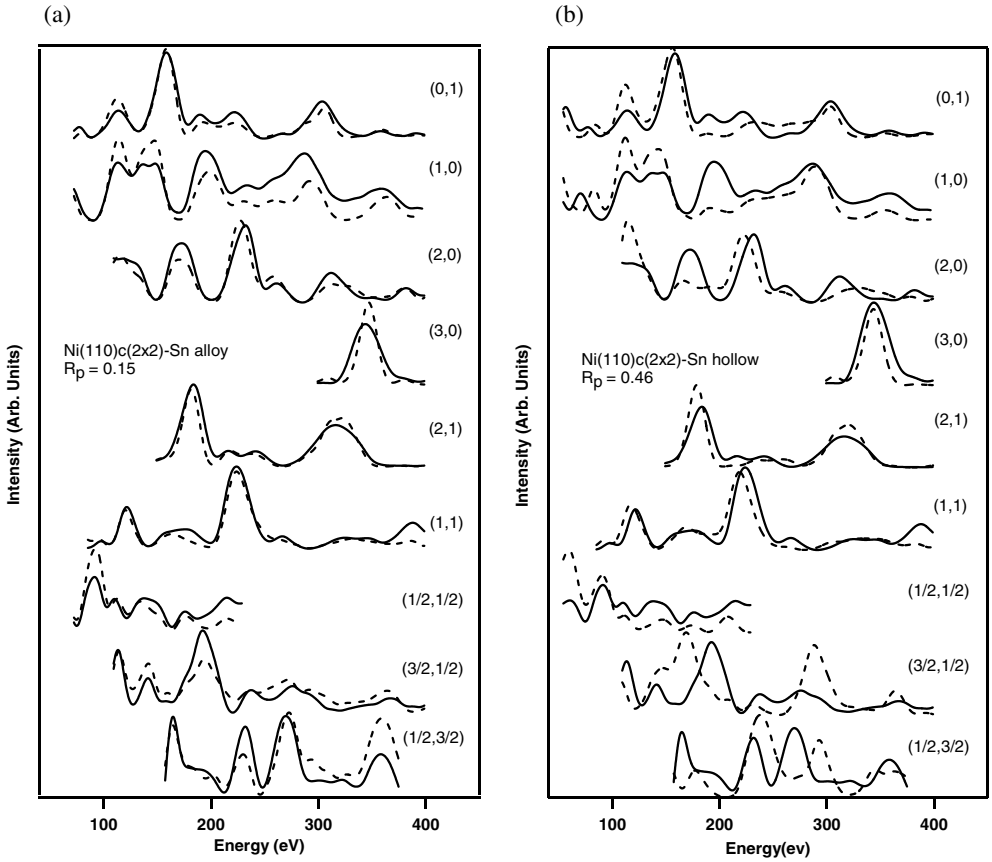

Figure 2. Comparison of experimental LEED intensity-energy spectra (full curves) for the Ni(110)$c(2\times2)$–Sn surface with the best-fit theoretical curves (dashed curves) for the substitutional alloy (a) and hollow-site overlayer (b) models. The intensity scale of each beam is set to the same maximum value.

Table 2. R-factor and structural parameter values for the substitutional alloy and hollow-site overlayer models giving the best fit to the MEIS data. $\sqrt{\langle u^2\rangle}$ are the rms vibrational amplitudes; the suffix 1 corresponds to the vibrations of the Sn overlayer for the hollow-site overlayer structure and to the vibrations of both Sn and Ni atoms in the outermost layer in the substitutional alloy model. Suffix 2 corresponds to the vibrations of the first complete Ni layer.

Model	R_χ	$z_{\mathrm{Sn-Ni}}$ (Å)	z_{12} (Å)	z_{23} (Å)	$\sqrt{\langle u_1^2\rangle}$ (Å)	$\sqrt{\langle u_2^2\rangle}$ (Å)
Substitutional	6.0	0.33 ± 0.06	1.22 ± 0.04	1.24 ± 0.04	0.137 ± 0.02	0.110 ± 0.01
Hollow	7.1	1.38 ± 0.16	1.37 ± 0.04	1.19 ± 0.04	0.240 ± 0.06	0.134 ± 015

MEIS analysis in terms of best-fit structures are summarized in table 2 and figure 4 for the two principle structural models of interest, the substitutional alloy and the hollow-site overlayer.

As seen in table 2, the MEIS analysis shows a slight preference for the substitutional alloy model, but the difference between the two R-factor values between the two models is quite small, and formally marginally significant. This difficulty of distinguishing between substitutional adsorption and overlayer adsorption in the same site which the next substrate layer atoms would occupy is one which we have remarked upon in the past in the context

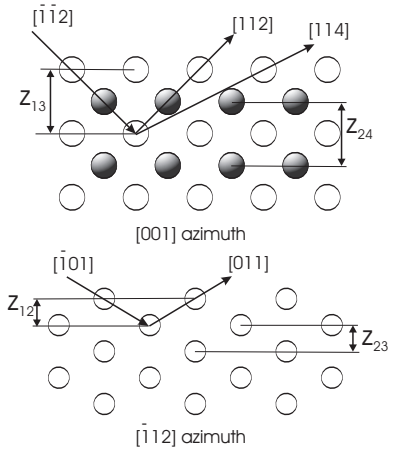

Figure 3. Side views of an ideally-terminated clean Ni(110) surface in the [001] and [$\bar{1}$12] azimuths showing the two different ion incidence geometries used in the MEIS study and some of the associated blocking directions. Shaded atoms are out of the plane of the page. Interlayer separations to which each scattering geometry is most sensitive are indicated.

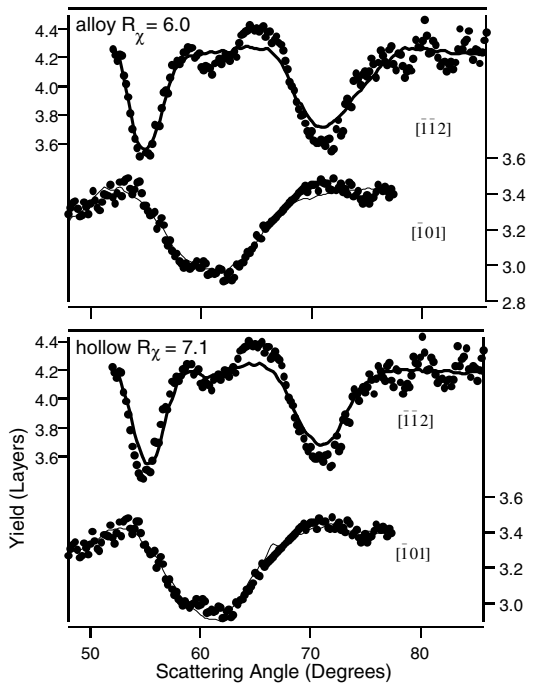

Figure 4. Comparison of MEIS experimental blocking curves (individual points) with the results of simulations for Ni(110)$c(2 \times 2)$–Sn surface for the substitutional alloy and hollow-site overlayer models. Associated structural parameters are summarized in table 2.

of fcc(111) surfaces [1, 10]. The problem arises because in both structures the adsorbate atoms have similar shadowing behaviour relative to the sub-surface layers, and differ only in terms of which layer is shadowed. Careful choice of the scattering geometry, however, can overcome this problem [1,2]. In view of the very clear distinction afforded by the LEED results,

however, more extensive MEIS experiments were not pursued. Notice, however, that even the limited amount of MEIS data used here provides essential confirmation of the main structural parameters of the substitutional alloy model, the differences between the values obtained from the two methods being within the estimated precision. In fact, further manual searches of the structural parameter space for the substitutional alloy revealed a local minimum in the R-factor for parameter values in even closer agreement with those of the LEED analysis, although the value of R at this minimum (6.3) was larger than the lowest global value (6.0); as the single-parameter precision estimates of the these two solutions overlap significantly, we give only the values for the global minimum in the table. Based on this unconstrained structural fitting, the MEIS analysis, in isolation, cannot exclude the hollow-site overlayer model, although the very large vibrational amplitudes of the Sn atoms found for this model, which are probably not physically reasonable, provide additional evidence that this is not the correct structural model. In addition, however, the optimum structural parameter values for the hollow-site overlayer model in LEED and MEIS, given in tables 1 and 2, are clearly in very poor agreement. This further reinforces the conclusion that this is not the correct structure; if the model is incorrect, the two techniques, which are based on quite different physical principles, can be expected to have to adjust the parameters values of the wrong model in wholly different ways to optimize the fit to experiment.

4. General discussion and conclusions

The primary conclusion of this study is that Sn on Ni(110), as on Ni(111) and Ni(100), adopts substitutional sites in the principal ordered sub-monolayer coverage phase. On all three faces there is also a significant degree of rumpling of the surface alloy layer, with the Sn atoms having larger spacings relative to the underlying complete Ni layer by amounts previously determined on Ni(111) [4] and Ni(100) [6] to be 0.46 ± 0.04 Å and 0.44 ± 0.05 Å respectively, while here for Ni(110) we find a value of 0.40 ± 0.03 Å from LEED and 0.33 ± 0.06 Å from MEIS. The Sn–Ni nearest-neighbour distances on these surfaces are thus 2.53 Å, 2.53 Å and 2.52 Å (or 2.51 Å on Ni(110) according to MEIS). These values are all significantly less than the values in the range 2.61–2.64 Å quoted for the bulk Ni_3Sn alloy [5], reinforcing the idea [1, 2] that there is some kind of surface effect influencing the effective size of the atoms in the surface alloy phase.

As discussed in the introduction, there are well-known consequences of the reduction of valence electron density in the outermost layer of a metal surface due to spill-over into the vacuum. The atoms in the surface layer try to find an environment with a higher valence electron density, which causes a reduction in the outermost layer spacing and the appearance of a tensile surface stress [21]. This effect is clearly most significant for a surface having a low atomic packing density, such as fcc(110), and is smallest on a surface of high atomic packing density, such as fcc(111). For the surface layer spacing contraction, this trend is well established. On fcc(111) surfaces, any surface layer spacing change is extremely small and experimental results are marginally significant. On fcc(100) surfaces, a small contraction (a few per cent) is commonly found, while on fcc(110) surfaces this contraction can be 10–15% or more [22, 23]. In the case of Ni(110) all the more recent measurements seem to indicate that this value is 8–9% [24–26]. In the case of the Ni/Sn surface alloy there is also a pronounced trend in the Ni nearest-neighbour coordination of the substitutional Sn atoms within the surface alloy layer across this series of surfaces, with six such neighbours on (111), four on (100) and only two on (110). The same trend, of course, occurs if we ignore the rumpling and include both surface layer and second layer neighbours giving coordination numbers of nine for (111), eight for (100) and six for (110), although the driving force to reduce the rumpling is presumably most strongly influenced by the number of nearest neighbours in the highly-rumpled state when the

second layer atoms are significantly further away, and by the lateral interactions which define the surface stress. We might therefore speculate that there should be a trend for the corrugation amplitude of the surface alloy layer to fall through this sequence of surface orientations. Of course, the effect is rather subtle, because the fact that the more open-packed (110) face shows the largest surface layer contraction might imply that there is less need for a reduction in the lateral atomic spacing as reflected in the tensile surface stress. Notice, in this context, that our data for the Ni(110)$c(2 \times 2)$–Sn surface alloy phase actually indicate that the contraction of the outermost (half-) layer is less than on the clean surface: LEED and MEIS give this contraction as 4 and 2% respectively.

An inspection of the various measurements of the Ni/Sn surface corrugation amplitude shows that there is, indeed, a trend of the type suggested here, although its statistical significance is marginal. If we take the LEED determination in the present experiments as more complete and thus more reliable, the best-fit values for (111), (100) and (110) of 0.46 Å, 0.44 Å and 0.40 Å, respectively, do show the suggested trend, but the differences are at the limits of the estimated precision. The lower (but formally consistent) value of 0.33 Å found in the MEIS study of the (110) face provides some indication that this trend may be real. Clearly this subtle issue lies at the limit of precision of current surface structural probes [23].

Acknowledgments

The authors would like to thank Professor M A Van Hove and Dr A Barbieri for supplying the PHASE SHIFT and SATLEED packages, and Dr E Soares and Dr A Wander for useful discussions. The financial support of the Physical Sciences and Engineering Research Council is gratefully acknowledged

References

[1] Brown D, Quinn P D, Woodruff D P, Bailey P and Noakes T C Q 2000 *Phys. Rev.* B **61** 7706
[2] Woodruff D P, Brown D, Quinn P D, Noakes T C Q and Bailey P 2001 *Nucl. Instrum. Methods* B **183** 128
[3] Overbury S H, Mullins D R, Paffett M T and Koel B E 1991 *Surf. Sci.* **254** 45
[4] Ku Y and Overbury S H 1992 *Surf. Sci.* **273** 341
[5] Overbury S H and Ku Y 1992 *Phys. Rev.* B **46** 7868
[6] Li Y D, Jiang L Q and Koel B E 1994 *Phys. Rev.* B **49** 2813
[7] Lee A F, Baddeley C J, Hardacre C, Morridge G D, Ormerod R M and Lambert R M 1998 *J. Phys. Chem.* B **101** 2797
[8] See http://www.dl.ac.uk/MEIS
[9] Brown D, Noakes T C Q, Woodruff D P, Bailey P and Le Goaziou Y 1999 *J. Phys.: Condens. Matter* **11** 1889
[10] Bailey P, Noakes T C Q and Woodruff D P 1999 *Surf. Sci.* **426** 358
[11] Van der Veen J F 1985 *Surf. Sci. Rep.* **5** 199
[12] Bailey P, Noakes T C Q, Baddeley C J, Tear S P and Woodruff D P 2001 *Nucl. Instrum. Methods* B **183** 62
[13] Van Hove M A, Moritz W, Over H, Rous P J, Wander A, Barbieri A, Materer N, Starke U and Somorjai G A 1993 *Surf. Sci. Rep.* **19** 191
[14] Barbieri A and Van Hove M A, private communication, http://electron.lbl.gov/leedpack
[15] Pendry J B 1980 *J. Phys. C: Solid State Phys.* **13** 937
[16] Frenken J W M, Tromp R M and van der Veen J F 1986 *Nucl. Instrum. Methods* B **17** 334
[17] Noakes T C Q, Bailey P and Woodruff D P 1998 *Nucl. Instrum. Methods* B **136–8** 1125
[18] Quinn P, Brown D, Woodruff D P, Noakes T C Q and Bailey P 2001 *Surf. Sci.* **491** 208
[19] Fletcher R 1987 *Practical Methods of Optimisation* 2nd edn (Chichester: Wiley)
[20] Gill P E, Murray W and Wright M H 1981 *Practical Optimisation* (London: Academic)
[21] See, for example, Ibach H 1997 *Surf. Sci. Rep.* **29** 193
[22] Watson P R, Van Hove M A and Hermann K 1999 *NIST Surface Structure Database, version 2: NIST Standard Reference Database 42* NIST, Gaithersburg,
[23] Woodruff D P 2002 *Surf. Sci.* **500** at press
[24] Adams D L, Petersen L E and Sorensen C S 1985 *J. Phys. C: Solid State Phys.* **18** 1753
[25] Yalisove S M, Graham W R, Adams E D, Copel M and Gustafsson T 1986 *Surf. Sci.* **171** 400
[26] Reimer W, Penka V, Skottke M, Behm R J, Ertl G and Moritz W 1987 *Surf. Sci.* **186** 45